Multi-modal, ultrasensitive, wide-range humidity sensing with Ti₃C₂ film

Journal:	*Nanoscale*
Manuscript ID	NR-ART-06-2018-005170.R2
Article Type:	Paper
Date Submitted by the Author:	27-Oct-2018
Complete List of Authors:	Muckley, Eric; Oak Ridge National Laboratory, Center for Nanophase Materials Science Naguib, Michael; Tulane University, Department of Physics and Engineering Physics Ivanov, Ilia; Oak Ridge National Laboratory, Center for Nanophase materials Science

Multi-modal, ultrasensitive, wide-range humidity sensing with Ti_3C_2 film

Eric S. Muckley[1*], Michael Naguib[2], Ilia N. Ivanov[1*]

[1]Center for Nanophase Materials Sciences, Oak Ridge National Laboratory, P.O. Box 2008, Oak Ridge, Tennessee 37831, USA
[2]Department of Physics and Engineering Physics, Tulane University, New Orleans, Louisiana 70118, USA

*Corresponding authors: Eric Muckley, muckleyes@ornl.gov; Ilia Ivanov, ivanovin@ornl.gov
Keywords: MXene, Ti_3C_2, humidity, QCM, sensing, dissipation

Abstract
Gravimetric, direct-current electrical, and electrical impedance sensing modes were used to measure response of high surface area 2D Ti_3C_2 MXene film to water vapor pressures spanning 3 orders of magnitude (20 mTorr - 20 Torr). The Ti_3C_2 film exhibited reproducible reversible response in 0.1%-95% relative humidity (RH) range with a detection limit of < 20 mTorr H_2O partial pressure (< 0.1% RH). DC electrical current-based sensing with 3 mV operating voltage and 0.8 pW power consumption was demonstrated. The highest normalized sensitivity was shown for gravimetric sensing modalities which scale with the overtone number, reaching highest sensitivity of about 12 Hz / % RH at the 9th crystal overtone (45 MHz oscillation).

Introduction

A new class of two-dimensional (2D) transition metal carbides and carbonitrides termed MXenes is being explored for use in a wide range of electrochemical applications[1]. Because of high surface area and tunable terminations/ion intercalants, MXenes have been investigated for chemical sensing of sodium nitrite[2], ammonia[3], glucose[4], and hydrogen peroxide[5]. The most widely-studied MXene to date, Ti_3C_2, exhibits strong hydrophilicity and high electrical conductivity[6]. Experimental and computational studies have confirmed the presence of mixed -OH, -O, and -F terminations in Ti_3C_2 films which provide hydrophilic sites for water adsorption[1, 7-12]. Although these properties make Ti_3C_2 MXene well-suited for relative humidity (RH) sensing, much research on the H_2O response of Ti_3C_2 has been limited to studies of ion-intercalated Ti_3C_2[6, 13]. Ghidiu et al. reported on effect of water on Ti_3C_2 structure but did not correlate mechano-structural response to electrical or functional response[14]. Come et al. showed that adsorption of water can lead to stiffening of Ti_3C_2 film due to formation of highly ordered water layers between Ti_3C_2 sheets[15] but did not relate this effect to sensing performance. Römer et al. reported a linear increase in Ti_3C_2 resistivity as RH increased from 15-80%[16].

Ghidiu et al. showed that K^+, Na^+, Li^+, Ca^{2+}-intercalated Ti_3C_2 undergoes an increase in basal spacing during water intercalation between 2D Ti_3C_2 sheets, and the amount of adsorbed water, referenced to the molecular weight of ion-intercalated $T_3C_2T_x$, does not depend on the nature of intercalated ion[6]. Shpigel et al. reported negligible viscoelastic changes of Ti_3C_2 film in air under low humidity conditions[17]. However, it remains unclear how adsorbed water influences viscoelastic behavior of Ti_3C_2 films, and dynamic range and detection limits for Ti_3C_2-based humidity sensors have not been thoroughly investigated. We showed previously that K^+ and Mg^{2+} ion intercalated Ti_3C_2 film exhibited electrical and gravimetric response to water vapor between 20% and 80% RH[13]. However, dynamic range, detection limits, reversibility, and long-term stability and repeatability of non-intercalated Ti_3C_2- humidity sensors were not investigated in detail. Here we present the results on correlation between gravimetric and electrical response of Ti_3C_2 films to humidity, addressing important question of detection limits, operable range, reversibility, and long-term stability/repeatability of Ti_3C_2-based gravimetric and electrical RH sensors. As evidenced by modeling of multi-frequency gravimetric response, Ti_3C_2 film exhibits a gradual transition from rigid to viscoelastic behavior as humidity increases.

Other 2D materials including VS_2[18], MoS_2[19], black phosphorus nanosheets[20] and graphene[21] exhibit strong response to water vapor but their operable range as RH sensors is tested only for RH > 10% (corresponding to ~3000 ppm H_2O partial pressure). Response to 1% RH has been observed in graphene[21], but sub-1% RH detection limits are

seldom reported. In this study, we demonstrate gravimetric response of Ti_3C_2 to 0.1% RH, corresponding to ~30 ppm H_2O partial pressure. We investigated the humidity range under which Ti_3C_2 film may be used for reversible RH sensing and probed detection limits for both gravimetric and electrical sensing modes. We used multi-harmonic quartz crystal microbalance with dissipation monitoring (QCM-D) to correlate Ti_3C_2 sensor response with viscoelastic behavior in the Ti_3C_2 film.

Experiment

Details of Ti_3AlC_2 synthesis were described elsewhere by Naguib et al.[22]. For synthesis of Ti_3C_2 used in this study, Ti_3AlC_2 was etched using a solution of LiCl dissolved in 10 wt% HF (1 g Ti_3AlC_2/10 mL of etching solution and Ti_3AlC_2/LiCl ~ 1:5 molar ratio) at room temperature for 24 hours. After etching, the mixture was centrifuged, the top liquids were decanted, fresh deionized water was added to the settled powder, then centrifuged, and the top liquids were decanted. The washing steps were repeated until the pH of the top liquids reached values > 5. Settled powder was then rinsed with 37% HCl (30 mL of 37% HCl: 1 g of powder) then centrifuged. Liquids were decanted and the rinsing process using HCl was repeated four times to remove extra salts from the etching process and to remove any intercalated Li ions and replace them with protons. This was followed by rinsing with deionized water. The wet powder was vacuum filtered to dry. Dry Ti_3C_2 was mixed with deionized water to produce 34% Ti_3C_2 by weight solution. For gravimetric and viscoelastic measurements, 1 μL of solution was drop-cast on pre-cleaned 5 MHz-resonant frequency AT-cut gold-coated quartz crystal microbalance (QCM) crystals. For electrical measurements, 1 μL of solution was drop-cast on undoped SiO_2 substrates with pre-patterned 2 μm-spaced gold interdigitated electrodes (for resistivity and passive sensing experiments) and pre-patterned 1 cm-spaced gold electrodes for impedance spectroscopy measurements. Deposition of Ti_3C_2 film resulted in a porous network of conductive pathways with up to ~5 μm thick (see Figure S1). All synthesis, preparation and experiments were conducted at room temperature.

For testing, Ti_3C_2-coated QCM and pre-pattered electrodes were placed under 10^{-4} Torr (1.33×10^{-7} bar) vacuum for 12 hours before exposure to water vapor. Fundamental QCM frequency shift was recorded using an openQCM Pierce oscillator circuit[23]. DC resistivity and passive current measurements were performed using a Keithley 2420 source-meter with 20 mV and 3 mV bias respectively. Electrochemical impedance spectroscopy (EIS) was performed using a Zahner IM6 electrochemical workstation. Humidity was controlled by injecting water vapor into the vacuum chamber at 20 cm^3/min flow rate using a mass flow controller at. A LabVIEW program was used to control the H_2O flow and record resistivity of the film and frequency shift of the QCM during the experiment. For viscoelasticity measurements, frequency and dissipation were recorded at 1st, 3rd, 5th, 7th, and 9th crystal harmonics for a Ti_3C_2-coated 5 MHz QCM crystal inside a KSV QCMZ-500 liquid flow cell while humidity was varied using an L&C RH-200 humidity generator with dry N_2 as a carrier gas.

Results and Discussion

DC resistive and gravimetric sensing modalities. Electrical resistance of Ti_3C_2 film (ΔR) and fundamental frequency shift (Δf) of Ti_3C_2-coated QCM were measured under changing RH conditions. When RH was increased from ~0% to 95%, frequency shift of the Ti_3C_2-coated QCM was ~50 times higher than that of the bare Au reference QCM (Figure 1a), indicating selective adsorption of H_2O on Ti_3C_2 likely due to its relatively high surface area (10-20 m^2/g) and hydrophilic surface-terminating functional groups (OH, O, and H)[1]. Values of Δf and ΔR were observed under H_2O partial pressures spanning a range of 3 orders of magnitude (20 mTorr – 20 Torr) (Figure 1(a) bottom panel). Gravimetric (Δf) and resistive (ΔR) responses decreased exponentially with RH (Figure 1(b)), indicating that the strongest RH response of Ti_3C_2 occurred under dry (< 20% RH) conditions. Previous experimental and theoretical results showed that adsorption of ~2 H_2O molecules per unit cell in ion-intercalated Ti_3C_2 resulted in significant structural and electrical changes[13]. The small electrical resistance change (~1.75 Ω) from 0-95% RH was ~0.8% of the total resistance of the film (~200 Ω), indicating that conductive Ti_3C_2 with small electrical response can still be effective as a wide-range RH sensing material.

To estimate detection limits of gravimetric- and resistive- Ti_3C_2 sensors, 30 second integration time was used to decrease signal to noise ratio (SNR). Increasing the integration time without loss of important temporal information was possible due to the slow H_2O response kinetics shown in Figure 1c. Upon exposure to a ~25 mTorr H_2O vapor pulse (corresponding to ~0.1% RH) (Figure 1(c) bottom panel), Ti_3C_2-coated QCM exhibited fundamental frequency shift of ~1.3 Hz/cm^2 corresponding to mass change of ~23 ng/cm^2 under Sauerbrey conditions[24], and electrical resistance of the Ti_3C_2 film increased by ~140 mΩ. Although the frequency shift and resistance change are

small compared to those reported for typical thin film resistive and QCM-based RH sensors[25-28], Δf and ΔR exhibited signal-to-noise ratios SNRs of ~5 in response to the 0.1% RH pulse which demonstrates that Ti_3C_2 may be used as a RH sensing material under an extremely broad range of humidity levels (0.1%-95% RH). While Δf and ΔR kinetics occurred over the scale of ~1 hour at RH > 20% (Figure 1(a)), change in Δf occurred over 1-2 hours and change in and ΔR occurred over a period of over 5 hours when RH was increased from 0.01% to 0.1%. This suggests that at low water vapor partial pressure, capillary action which drives H_2O diffusion between individual 2D Ti_3C_2 layers is severely limited[13].
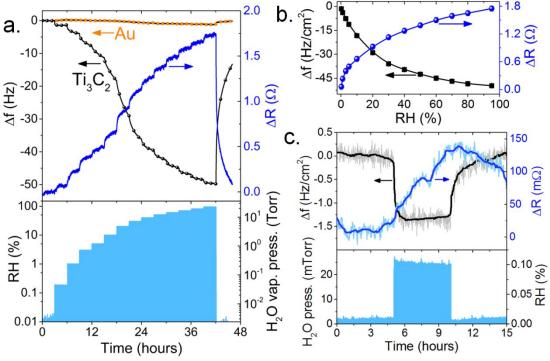

Figure 1. (a) Top panel: Fundamental frequency shift (Δf, left axis) of Ti_3C_2-coated QCM and bare Au-coated QCM during exposure to water vapor partial pressures spanning over 3 orders of magnitude (bottom panel). Right axis of top panel shows DC electrical resistance change (ΔR) of Ti_3C_2 film. Water concentration in bottom panel is shown in terms of relative humidity (RH) and H_2O vapor pressure. (b) Fundamental frequency shift (black, left axis) and electrical resistance change (blue, right axis) measured from 0-95% RH after 3 hours of exposure to each RH level. (c) Frequency shift and resistance change during exposure to single H_2O vapor pulse (bottom panel) corresponding to ~25 mTorr H_2O vapor pressure (0.1% RH). Solid dark lines show response after 50-point adjacent averaging.

To probe long-term sensor stability and reproducibility, gravimetric response of the Ti_3C_2 film was recorded during repeated cycling from 20% to 80% RH. After 20 cycles over a duration of 18 hours (Figure S2(a)), the film showed repeatable response within 6% (Figure S2(b)). Long-term stability of the film was probed by exposing sensor to constant RH level for 12 hours steps and recording resonant frequency of the Ti_3C_2-coated QCM. Gravimetric response of the film was stable to within 6% over a period of 12 hours (Figure S2(c))."

Frequency-dependent electric sensing modality. To investigate the mechanism of electrical response of Ti_3C_2 to water, electrical impedance spectroscopy (Z) was measured from 100 Hz – 4 MHz using 20 mVAC excitation with 0 VDC bias at 0, 5, 20, 40, 60, 80, and 95% RH. The effect of RH on impedance was most pronounced at low frequency (100 Hz) (Figure S3(a)), followed a roughly exponential increase with RH (Figure S3(b)), and showed ~100% reversibility after water vapor was removed (Figure 2(a)) from the measurement chamber, in agreement with RH-dependent DC resistivity measurements. The semi-circle in the Nyquist plot (Figure 2(b)) is a signature of combined effects of resistive (R) and capacitive (C) elements, which may be modeled by an equivalent double RC circuit (shown in inset of Figure 2(b)) composed of contact resistance (R_C), resistance and capacitance associated with conduction through Ti_3C_2 grains (R_G and C_G respectively), and resistance and capacitance associated with conduction across grain boundaries (R_{GB} and C_{GB} respectively)[29]. The dominance of a single semi-circle in the

Nyquist plot, along with the high conductivity of Ti_3C_2[30], suggests that the majority of resistance and capacitance is associated with conduction across grain boundaries while bulk Ti_3C_2 grains contribute insignificantly to the film impedance. The resistive (Figure 2c) and capacitive (Figure 2d) values of equivalent circuit parameters demonstrate that while impedance of the conductive bulk grains changed insignificantly during RH exposure, both R_{GB} and C_{GB} increased with RH. RH-dependence of R_{GB} and C_{GB} closely resembled that of Z and DC electrical resistance which suggests that water accumulation near gain boundaries is the primary mechanism underlying Ti_3C_2 electrical response to water. The value of R_C which is generally associated with conduction at film domain-electrode junctions[31] showed a slight increase with RH (Figure S3c), indicating a voltage drop due to accumulation of adsorbed water at gold-Ti_3C_2 junctions. X-ray diffraction patterns (not shown) revealed no significant difference between dry Ti_3C_2 and Ti_3C_2 exposed to water, suggesting that that H_2O molecules did not intercalate between individual 2D Ti_3C_2 sheets, as expected.
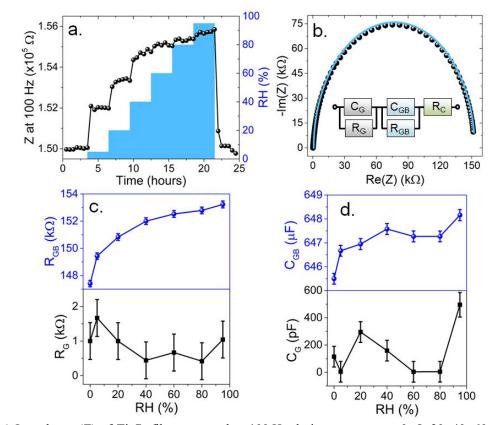

Figure 2. (a) Impedance (Z) of Ti_3C_2 film measured at 100 Hz during exposure to 0, 5, 20, 40, 60, 80, 95% RH (blue, right axis). (b) Nyquist representation of impedance of Ti_3C_2 film (black points) fitted to double RC equivalent circuit (blue line). Inset shows equivalent circuit model composed resistance and capacitance in bulk grains (R_G, C_G), resistance and capacitance at grain boundaries (R_{GB}, C_{GB}), and resistance at contacts (R_c). (c) Values of R_{GB} and R_G extracted from equivalent circuit fits. (d). Values of C_{GB} and C_G extracted from equivalent circuit fits. Error bars correspond to uncertainty introduced during fitting of equivalent circuit model.

Low-power current sensing modality. Low electrical resistivity (~20 $\Omega \cdot cm$) and strong response to water vapor enabled passive Ti_3C_2-based RH sensing with negligible power consumption. We applied constant 3 mV DC bias across Ti_3C_2 film and monitored picoamp-scale changes in electrical current (ΔI) under changing RH conditions (Figure 3(a)). Current decreased by ~260 pA when RH increased from 0-95% and showed reversible, reproducible response to changing RH conditions as RH was cycled from 0, 40, 95% and back to 0%. SNR in electrical current response is ~5 during response to 40% RH and ~7 during response to 95% RH, which enable ~10% RH resolution by passive (~3 mV) sensors in the 0-95% RH range. The value of ΔI followed a roughly double exponential trend with RH (Figure 3(b)), in agreement with low-frequency impedance and DC electrical resistance measurements. The 3 mV operational voltage is small enough to be supplied by entirely passive energy-harvesting devices including radio-frequency identification (RFID) antennas[32], vibrational micro-generators[33], and piezoelectric fabrics and

textiles[34]. Total power consumption of the 3 mV × 260 pA sensor is ~0.8 pW which is roughly the average power consumption of a human cell. The inset of Figure 3(b) shows that current-voltage characteristics of the Ti_3C_2 film from -1 to 1 V DC bias are linear, which suggests that passive RH sensors which rely on ambient energy harvesting devices may maintain linear current response even under variable power conditions.
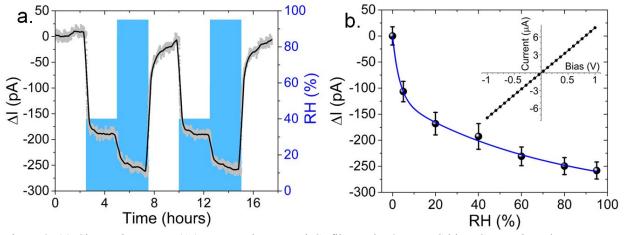

Figure 3. (a) Change in current (ΔI) measured across Ti_3C_2 film under 3 mV DC bias. Gray points show measured current, black line shows current after smoothing by 50-point adjacent averaging. Blue pulses (right axis) correspond to 0, 40, and 95% RH. (b) Current change showed roughly double exponential trend with RH (blue line). Error bars represent amplitude of noise in current signal. Inset: Ti_3C_2 film showed linear current-voltage characteristics from -1 to 1 VDC bias.

Mechanism of gravimetric response to water vapor. We used quartz crystal microbalance with dissipation monitoring (QCM-D) for probing frequency shift (Δf) and dissipation change (ΔD) of Ti_3C_2-coated QCM at 1st, 3rd, 5th, 7th and 9th crystal harmonics to investigate whether exposure to high humidity conditions caused any observable viscoelastic changes in the sensing film. A thin homogenous film rigidly-bound to the QCM surface undergoes frequency shift which is proportional to mass change in accordance with the Sauerbrey equation[24]. Under Sauerbrey conditions, Δf and ΔD are harmonic-independent and thus show negligible variation between harmonics after normalization to harmonic number[35]. This was observed in QCM-D measurements performed on a bare Au-coated QCM from 5%-90% RH (Figure S4), which indicated that changes in resonant frequency of the bare Au crystal were strictly a result of mass loading of the resonator.

The QCM coated with Ti_3C_2 film exhibited significant harmonic-dependent frequency shift and dissipation change in response to changing RH (Figure S5), indicating viscoelastic change in the Ti_3C_2 film[35]. The frequency shift and dissipation change during H_2O adsorption on bare Au were subtracted from Δf and ΔD values measured on the Ti_3C_2-coated crystal to remove the effects of changing density and viscosity of humid air and to isolate the effect of water on viscoelastic response of Ti_3C_2. Normalized $\Delta f/n$ and $\Delta D/n$ (where n is harmonic number) shown in Figure 4(a) and S5 respectively exhibited harmonic-dependence which increased with increasing RH. The slope $\Delta D/\Delta f$ was used to estimate energy dissipation per unit mass of the Ti_3C_2 film[36] (Figure S6). Significant deviations from the linear relationship between ΔD and Δf generally occurred near 50% RH (Figure S6), which suggests the onset of structural/conformational changes, viscoelastic changes, or interface slip between Ti_3C_2 film and the gold electrode[13-14, 30-31].

The simplest way to account for nonlinear mass loading of the resonator is to treat the film/water adlayer as a viscous liquid using the Kanazawa-Gordon equation[37]: $\Delta f = f_0^{3/2}(\rho\eta/\pi\mu_q\rho_q)^{1/2}$, where ρ and η are density and absolute viscosity of the effective liquid and μ_q and ρ_q are shear modulus and density of the quartz resonator. We used frequency shift of the fundamental resonant frequency (Δf_1) to estimate the corresponding Sauerbrey frequency shifts at higher harmonics by scaling Δf_1 linearly with harmonic number[35]. The deviation between Sauerbrey frequency shift (Δf_S) and experimentally-measured frequency shift (Δf_{exp}) was used to estimate the frequency shift resulting from viscoelastic changes in the adlayer film as described by Kanazawa (Δf_K), so that $\Delta f_{exp} = \Delta f_S + \Delta f_K$ (Figure S8). Using Δf_K and the Kanazawa-Gordon equation, we obtained estimates for $\Delta\eta\rho$, the change in product of effective viscosity and density of the Ti_3C_2 adlayer film under changing RH conditions (Figure 4(b)). The value of

Δηρ increased with RH as water filled in pores in the Ti_3C_2 film and increased the average density. It is expected that the effective viscosity of the Ti_3C_2 adlayer increased with RH due to softening of the film by water. Water accumulation near Ti_3C_2 surfaces may disrupt van der Waals interactions between adjacent Ti_3C_2 domains, decreasing rigidity of the film and contributing to energy damping observed in measurements of ΔD. The ratio $\Delta f_K / \Delta f_S$ which compares the importance of viscoelastic effects to mass loading effects generally increases with RH (Figure S9). Higher order harmonics typically probe regions of the adlayer film which are closer to the crystal surface, since penetration depth of the acoustic wave into the adlayer film scales as $\sqrt{1/f}$.[38] We performed additional viscoelastic modelling of the Ti_3C_2 film using the approach of Voinova et al.[39] as described in the supporting information. The results suggest that viscoelastic effects are most pronounced close to the Ti_3C_2/crystal interface. This is consistent with results from electrical impedance modelling which suggest that water accumulation at Ti_3C_2/crystal interface led to changes in charge transfer resistance. Notably, observed viscoelastic change in the Ti_3C_2 film did not result in unpredictable behavior in gravimetric or electrical response of Ti_3C_2 to water, which suggests that Ti_3C_2 film may be used for wide-range RH sensing even under extreme RH conditions which induce viscoelastic changes in the film.
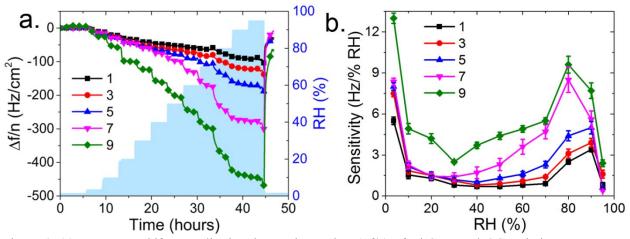

Figure 4. (a) Frequency shift normalized to harmonic number (Δf/n) of Ti_3C_2-coated QCM during exposure to increasing RH levels (blue, right axes). Values of Δf/n for bare Au QCM (Figure S4) were subtracted to remove effects of water adsorption on Au and drag forces arising from changing density and viscosity of humid air. Legend shows crystal harmonic number. (b) Sensitivity of Ti_3C_2 film to humidity (gravimetric) estimated as a ratio of normalized frequency shift of 1st, 3rd, 5th, 7th and 9th harmonics over change in RH%.

We compared sensitivity of all modalities using normalized sensitivity approach (Figure 5). Sensitivity of each sensing modality was first estimated as a slope of response over a given RH change and plotted against relative humidity, Figure S12. Then, the sensitivity was normalized to maximum of sensitivity for each modality. Majority of sensing modalities have similar normalized sensitivity for low range of humidifies and smaller for mid and high humidity. The advantage of gravimetric over other sensing modalities is apparent and the 7th harmonic showing the best sensitivity over full humidity range.
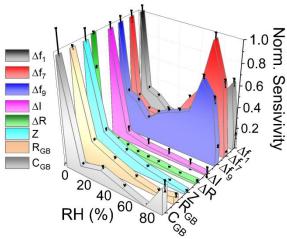
Figure 5. Normalized sensitivity of each sensing mode. Normalized sensitivity = S/S_{max}, where S is sensitivity in units shown in (Fig. b), and S_{max} is maximum sensitivity achieved for a given sensing mode.

Conclusions

We tested several reversible water sensing modes using Ti_3C_2 thin film. These modalities include multi-frequency gravimetric, DC-resistive, and frequency-dependent electrical response to adsorption of water from 20 mTorr H_2O partial pressure (0.1% RH) to 95% RH. Modelling of electrical impedance revealed that the primary mechanism behind electrical response of Ti_3C_2 was related to charge transfer resistance of the film due to adsorbed water at Ti_3C_2-electrode interfaces. Low power DC resistance sensing modality was demonstrated at 3 mV operating voltage that could potentially be supplied by a passive energy-harvesting device. Using multi-harmonic QCM-D and modelling of Ti_3C_2 viscoelastic RH response, we showed that density and/or viscosity of the film increased during adsorption of water. Changes in viscoelastic properties of the film did not prevent reversible RH sensing behavior under the wide range of H_2O partial pressures which were probed. Among all tested modalities, the highest normalized sensitivity was shown for gravimetric sensing modalities.
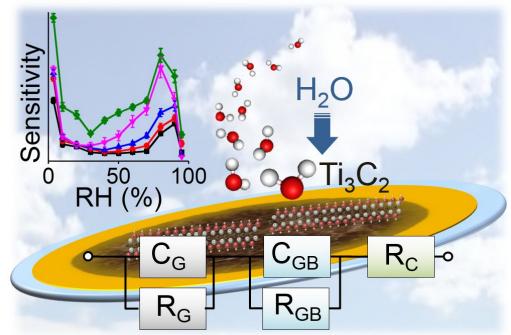
Acknowledgement

References

1.   Naguib, M.; Mochalin, V. N.; Barsoum, M. W.; Gogotsi, Y., 25th Anniversary Article: Mxenes: A New Family of Two-Dimensional Materials. *Advanced Materials* **2014,** *26* (7), 992-1005.
2.   Liu, H.; Duan, C.; Yang, C.; Shen, W.; Wang, F.; Zhu, Z., A Novel Nitrite Biosensor Based on the Direct Electrochemistry of Hemoglobin Immobilized on Mxene-Ti_3C_2. *Sensors and Actuators B: Chemical* **2015,** *218*, 60-66.
3.   Xiao, B.; Li, Y.-c.; Yu, X.-f.; Cheng, J.-b., Mxenes: Reusable Materials for NH_3 Sensor or Capturer by Controlling the Charge Injection. *Sensors and Actuators B: Chemical* **2016,** *235*, 103-109.
4.   Rakhi, R.; Nayak, P.; Xia, C.; Alshareef, H. N., Novel Amperometric Glucose Biosensor Based on Mxene Nanocomposite. *Scientific reports* **2016,** *6*, 36422.

5. Lorencová, L.; Bertok, T.; Dosekova, E.; Holazová, A.; Paprckova, D.; Vikartovská, A.; Sasinková, V.; Filip, J.; Kasák, P.; Jerigová, M., Electrochemical Performance of $Ti_3C_2T_x$ Mxene in Aqueous Media: Towards Ultrasensitive H_2O_2 Sensing. *Electrochimica Acta* **2017,** *235*, 471-479.

6. Ghidiu, M.; Halim, J.; Kota, S.; Bish, D.; Gogotsi, Y.; Barsoum, M. W., Ion-Exchange and Cation Solvation Reactions in Ti_3C_2 Mxene. *Chemistry of Materials* **2016,** *28* (10), 3507-3514.

7. Hope, M. A.; Forse, A. C.; Griffith, K. J.; Lukatskaya, M. R.; Ghidiu, M.; Gogotsi, Y.; Grey, C. P., NMR Reveals the Surface Functionalisation of Ti_3C_2 Mxene. *Physical Chemistry Chemical Physics* **2016,** *18* (7), 5099-5102.

8. Anasori, B.; Lukatskaya, M. R.; Gogotsi, Y., 2D Metal Carbides and Nitrides (Mxenes) for Energy Storage. *Nature Reviews Materials* **2017,** *2* (2), 16098.

9. Lei, J.-C.; Zhang, X.; Zhou, Z., Recent Advances in Mxene: Preparation, Properties, and Applications. *Frontiers of Physics* **2015,** *10* (3), 276-286.

10. Xie, Y.; Kent, P., Hybrid Density Functional Study of Structural and Electronic Properties of Functionalized $Ti_{n+1}X_n$ (X= C, N) Monolayers. *Physical Review B* **2013,** *87* (23), 235441.

11. Berdiyorov, G., Optical Properties of Functionalized $Ti_3C_2T_2$ (T= F, O, OH) Mxene: First-Principles Calculations. *Aip Advances* **2016,** *6* (5), 055105.

12. Ng, V. M. H.; Huang, H.; Zhou, K.; Lee, P. S.; Que, W.; Xu, J. Z.; Kong, L. B., Recent Progress in Layered Transition Metal Carbides and/or Nitrides (Mxenes) and Their Composites: Synthesis and Applications. *Journal of Materials Chemistry A* **2017,** *5* (7), 3039-3068.

13. Muckley, E. S.; Naguib, M.; Wang, H.-W.; Vlcek, L.; Osti, N. C.; Sacci, R. L.; Sang, X.; Unocic, R. R.; Xie, Y.; Tyagi, M., Multimodality of Structural, Electrical, and Gravimetric Responses of Intercalated Mxenes to Water. *ACS Nano* **2017**.

14. Ghidiu, M.; Kota, S.; Drozd, V.; Barsoum, M. W., Pressure-Induced Shear and Interlayer Expansion in Ti_3C_2 Mxene in the Presence of Water. *Science Advances* **2018,** *4* (1), eaao6850.

15. Come, J.; Xie, Y.; Naguib, M.; Jesse, S.; Kalinin, S. V.; Gogotsi, Y.; Kent, P. R.; Balke, N., Nanoscale Elastic Changes in 2D $Ti_3C_2T_x$ (Mxene) Pseudocapacitive Electrodes. *Advanced Energy Materials* **2016,** *6* (9).

16. Römer, F. M.; Wiedwald, U.; Strusch, T.; Halim, J.; Mayerberger, E.; Barsoum, M. W.; Farle, M., Controlling the Conductivity of Ti_3C_2 Mxenes by Inductively Coupled Oxygen and Hydrogen Plasma Treatment and Humidity. *RSC Advances* **2017,** *7* (22), 13097-13103.

17. Shpigel, N.; Lukatskaya, M. R.; Sigalov, S.; Ren, C. E.; Nayak, P.; Levi, M. D.; Daikhin, L.; Aurbach, D.; Gogotsi, Y., In Situ Monitoring of Gravimetric and Viscoelastic Changes in 2D Intercalation Electrodes. *ACS Energy Letters* **2017,** *2* (6), 1407-1415.

18. Feng, J.; Peng, L.; Wu, C.; Sun, X.; Hu, S.; Lin, C.; Dai, J.; Yang, J.; Xie, Y., Giant Moisture Responsiveness of VS_2 Ultrathin Nanosheets for Novel Touchless Positioning Interface. *Advanced Materials* **2012,** *24* (15), 1969-1974.

19. Zhang, D.; Sun, Y. e.; Li, P.; Zhang, Y., Facile Fabrication of MoS_2-Modified SnO_2 Hybrid Nanocomposite for Ultrasensitive Humidity Sensing. *ACS Applied Materials & Interfaces* **2016,** *8* (22), 14142-14149.

20. Erande, M. B.; Pawar, M. S.; Late, D. J., Humidity Sensing and Photodetection Behavior of Electrochemically Exfoliated Atomically Thin-Layered Black Phosphorus Nanosheets. *ACS Applied Materials & Interfaces* **2016,** *8* (18), 11548-11556.

21. Smith, A. D.; Elgammal, K.; Niklaus, F.; Delin, A.; Fischer, A. C.; Vaziri, S.; Forsberg, F.; Råsander, M.; Hugosson, H.; Bergqvist, L., Resistive Graphene Humidity Sensors with Rapid and Direct Electrical Readout. *Nanoscale* **2015,** *7* (45), 19099-19109.

22. Naguib, M.; Kurtoglu, M.; Presser, V.; Lu, J.; Niu, J.; Heon, M.; Hultman, L.; Gogotsi, Y.; Barsoum, M. W., Two-Dimensional Nanocrystals Produced by Exfoliation of Ti_3AlC_2. *Advanced Materials* **2011,** *23* (37), 4248-4253.

23. Muckley, E. S.; Anazagasty, C.; Jacobs, C. B.; Hianik, T.; Ivanov, I. N. In *Low-Cost Scalable Quartz Crystal Microbalance Array for Environmental Sensing*, SPIE Organic Photonics+ Electronics, International Society for Optics and Photonics: **2016**; pp 99440Y-99440Y-8.

24. Sauerbrey, G., Verwendung Von Schwingquarzen Zur Wägung Dünner Schichten Und Zur Mikrowägung. *Zeitschrift für physik* **1959,** *155* (2), 206-222.

25. Muckley, E. S.; Miller, N.; Jacobs, C. B.; Gredig, T.; Ivanov, I. N., Morphology-Defined Interaction of Copper Phthalocyanine with O_2/H_2O. *Journal of Photonics for Energy* **2016,** *6* (4), 045501-045501.

26. Muckley, E. S.; Nelson, A. J.; Jacobs, C. B.; Ivanov, I. N., Multimodal Probing of Oxygen and Water Interaction with Metallic and Semiconducting Carbon Nanotube Networks under Ultraviolet Irradiation. *Journal of Photonics for Energy* **2016,** *6* (2), 025506-025506.

27. Muckley, E. S.; Jacobs, C. B.; Vidal, K.; Mahalik, J. P.; Kumar, R.; Sumpter, B. G.; Ivanov, I. N., New Insights on Electro-Optical Response of Poly (3, 4-Ethylenedioxythiophene): Poly (Styrenesulfonate) Film to Humidity. *ACS Applied Materials & Interfaces* **2017,** *9* (18), 15880-15886.

28. Muckley, E. S.; Jacobs, C. B.; Vidal, K.; Lavrik, N. V.; Sumpter, B. G.; Ivanov, I. N., Multi-Mode Humidity Sensing with Water-Soluble Copper Phthalocyanine for Increased Sensitivity and Dynamic Range. *Scientific reports* **2017,** *7* (1), 9921.

29. Jacobs, C. B.; Maksov, A. B.; Muckley, E. S.; Collins, L.; Mahjouri-Samani, M.; Ievlev, A.; Rouleau, C. M.; Moon, J.-W.; Graham, D. E.; Sumpter, B. G., UV-Activated ZnO Films on a Flexible Substrate for Room Temperature O_2 and H_2O Sensing. *Scientific reports* **2017,** *7* (1), 6053.

30. Kurtoglu, M.; Naguib, M.; Gogotsi, Y.; Barsoum, M. W., First Principles Study of Two-Dimensional Early Transition Metal Carbides. *Mrs Communications* **2012,** *2* (4), 133-137.

31. Alavi, S. M. M.; Mahdi, A.; Payne, S. J.; Howey, D. A., Identifiability of Generalized Randles Circuit Models. *IEEE Transactions on Control Systems Technology* **2017,** *25* (6), 2112-2120.

32. Orecchini, G.; Yang, L.; Tentzeris, M.; Roselli, L. In *Wearable Battery-Free Active Paper Printed Rfid Tag with Human-Energy Scavenger*, Microwave Symposium Digest (MTT), 2011 IEEE MTT-S International, IEEE: **2011**; pp 1-4.

33. Paradiso, J. A.; Starner, T., Energy Scavenging for Mobile and Wireless Electronics. *IEEE Pervasive computing* **2005,** *4* (1), 18-27.

34. Swallow, L.; Luo, J.; Siores, E.; Patel, I.; Dodds, D., A Piezoelectric Fibre Composite Based Energy Harvesting Device for Potential Wearable Applications. *Smart Materials and Structures* **2008,** *17* (2), 025017.

35. Cho, N.-J.; Kanazawa, K. K.; Glenn, J. S.; Frank, C. W., Employing Two Different Quartz Crystal Microbalance Models to Study Changes in Viscoelastic Behavior Upon Transformation of Lipid Vesicles to a Bilayer on a Gold Surface. *Analytical Chemistry* **2007,** *79* (18), 7027-7035.

36. Tsortos, A.; Papadakis, G.; Gizeli, E., Shear Acoustic Wave Biosensor for Detecting DNA Intrinsic Viscosity and Conformation: A Study with QCM-D. *Biosensors and Bioelectronics* **2008,** *24* (4), 836-841.

37. Kanazawa, K. K.; Gordon, J. G., Frequency of a Quartz Microbalance in Contact with Liquid. *Analytical Chemistry* **1985,** *57* (8), 1770-1771.

38. Speller, N. C.; Siraj, N.; Regmi, B. P.; Marzoughi, H.; Neal, C.; Warner, I. M., Rational Design of QCM-D Virtual Sensor Arrays Based on Film Thickness, Viscoelasticity, and Harmonics for Vapor Discrimination. *Analytical Chemistry* **2015,** *87* (10), 5156-5166.

39. Voinova, M. V.; Rodahl, M.; Jonson, M.; Kasemo, B., Viscoelastic Acoustic Response of Layered Polymer Films at Fluid-Solid Interfaces: Continuum Mechanics Approach. *Physica Scripta* **1999,** *59* (5), 391.

TOC figure:

MXene (Ti_3C_2)-based humidity sensor demonstrates exceptional sensitivity to water vapor from 0.1%-95% RH with < 20 mTorr H_2O detection limit.